A statistical state dynamics-based analysis of the physical mechanisms sustaining and regulating turbulence in Couette flow

Brian F. Farrell
School of Engineering and Applied Science, Harvard University

Petros J. Ioannou*
Department of Physics, National and Kapodistrian University of Athens

(Dated: April 4, 2017)

This paper describes a study of the self-sustaining process in wall-turbulence. The study is based on a second order statistical state dynamics model of Couette flow in which the state variables are the streamwise mean flow (first cumulant) and perturbation covariance (second cumulant). This statistical state dynamics model is closed by either setting the third cumulant to zero or by replacing it with a stochastic parameterization. Statistical state dynamics models with this form are referred to as S3T models. S3T models have been shown to self-sustain turbulence with a mean flow and second order perturbation structure similar to that obtained by direct numerical simulation of the equations of motion. The use of a statistical state dynamics model to study the physical mechanisms underlying turbulence has important advantages over the traditional approach of studying the dynamics of individual realizations of turbulence. One advantage is that the analytical structure of statistical state dynamics isolates and directly expresses the interaction between the coherent mean flow and the incoherent perturbation components of the turbulence. Isolation of the interaction between these components reveals how this interaction underlies both the maintenance of the turbulence variance by transfer of energy from the externally driven flow to the perturbation components as well as the enforcement of the observed statistical mean turbulent state by feedback regulation between the mean and perturbation fields. Another advantage of studying turbulence using statistical state dynamics models is that the analytical structure of S3T turbulence can be completely characterized. For example, turbulence in the S3T system is demonstrably maintained by a parametric growth mechanism in which the fluctuation of the mean flow parametrically destabilize the incoherent component of the turbulence while in turn these perturbations maintain the mean flow fluctuations in a synergetic interaction. Furthermore, the equilibrium statistical state of the turbulence can be demonstrated to be enforced by feedback regulation in which transient growth of the incoherent perturbations episodically suppresses coherent streak growth preventing runaway parametric growth of the incoherent turbulent component. Using S3T to isolate these parametric growth and feedback regulation mechanisms allows a detailed characterization of the dynamics of the self-sustaining process in S3T turbulence with compelling implications for understanding the mechanism of wall-turbulence.

I. INTRODUCTION

In this work the mechanisms sustaining and regulating wall-turbulence are studied. Understanding how the turbulent state is sustained against dissipation requires identifying the mechanism by which energy is systematically transferred from the externally driven flow to the turbulent fluctuations in the absence of fast inflectional instability of the mean velocity profile. Understanding how the turbulence is enforced to assume the observed statistical structure requires understanding the mechanism by which interaction between the mean and perturbation fields establishes and enforces this observed statistical state.

The ubiquitous roll-streak structure, which was first identified in the buffer layer [1], is known to play a key role in the dynamics of wall-turbulence. While the roll-streak structure is stable in plane wall-bounded flows, it is associated with rapid transient growth that produces robust energy transfer from the mean shear flow to the perturbation field when an optimally configured perturbation is excited [2, 3]. This growth results from a streamwise roll circulation giving rise to a streamwise streak through the lift-up mechanism [4]. What is not understood is how this mechanism is maintained in the absence of a linear instability. An early proposed resolution of this conundrum was that these structures participate in a regeneration cycle in which new streaks arise from perturbations the origin of which is ascribed to the break-up of previously formed streaks [5, 6]. This proposed cycle can be viewed as a nonlinear instability mechanism in which turbulence is sustained by energy transfer from the externally forced shear to the perturbation field due to the linear non-normal lift-up growth processes while this non-normal growth is in turn sustained by the continual re-emergence from the debris of the roll-streak structures by the perturbation–perturbation advective nonlinearity. Alternative mechanisms by which perturbation nonlinearity could sustain transient growth of the roll-streak structure have been the subject of study since this nonlinear basis of the instability maintaining wall-turbulence was postulated. Here we refer to these mechanisms col-

* pjioannou@phys.uoa.gr

lectively as self-sustaining processes.

An alternative to the regeneration cycle class of self-sustaining process is based on spanwise inflection of the streak velocity profile giving rise to an unstable, or at statistical equilibrium a neutral, eigenmode. In this class of self-sustaining process Reynolds stresses arrising from this eigenmode sustain the roll circulation [7–10]. However, subsequent work indicated that streaks are generally too weak to be robustly unstable and an alternative self-sustaining process was postulated in which transient growth rather than modal instability maintains the perturbations that force the roll [11]. An advantage of the transient growth self-sustaining process is that the optimal perturbations maximally exploit the energy of the wall-normal shear in addition to the spanwise shear that primarily supports the inflectional instability. In fact, the most rapidly growing perturbations in shear flow are oblique waves which optimally exploit, by lift-up, the large reservoir of energy in the wall-normal shear [12]. Moreover, the Reynolds stresses arising in association with these optimally growing oblique waves have been shown to give rise to the strong systematic forcing of the roll circulations required to maintain the streak [13] and consistently, oblique waves are commonly observed to accompany streaks in wall-turbulence [11].

While these various self-sustaining process mechanisms address the question of how the roll-streak structure might be destabilized by nonlinearity, they leave open the question of how this instability is regulated to zero mean growth and more generally how the turbulence is enforced to assume the observed statistical equilibrium state. Both of these questions can be addressed using the methods of statistical state dynamics and to this end we previously studied the self-sustaining process using a statistical state dynamics model [13, 14]. While analyzing complex spatially and temporally varying fields arising in observations and simulations of turbulent systems using statistical quantities is common practice, it is less common to adopt statistical variables directly as the variables for expressing the dynamics of the turbulent system. An early attempt to exploit the potential of employing statistical state dynamics to provide insight into turbulence involved formal expansion and closure of the Navier-Stokes equations in cumulants [15–17]. The cumulant method was subsequently restricted in application in part due to the difficulty of obtaining robust closure of the expansion when it was applied to isotropic homogeneous turbulence. Surprisingly, while the assumed vanishing of the first cumulant in isotropic homogeneous turbulence would appear to simplify the dynamics, subsequent experience in solving statistical state dynamics models in the cases of anisotropic two dimensional beta-plane turbulence [18–21] and turbulent convection [22, 23] revealed that closures retaining nontrivial expressions for both but only the first and second cumulants comprised the entire essential dynamics of the turbulence. For example, statistical state dynamics of beta-plane turbulence closed at second order predicts the equilibrium state of this turbulence to be an analytical solution (in the form of a fixed point) of the nonlinear statistical state dynamics including the remarkable spontaneous formation of jets with the observed structure containing as much as 90% of the kinetic energy of the flow [18–20, 24–28]. In retrospect, precedence for such a program was provided by the work of Herring [22, 23] in his study of the statistical equilibrium of turbulent convection. The approach of using second order statistical state dynamics to obtain the statistical equilibrium state of turbulent convection has its roots in Malkus's theory in which the statistical state was sought as the fixed point equilibrium between the mean thermal structure and the turbulent heat fluxes [29, 30]. The success of this program in providing an explanation for the statistical mean state of turbulent convection was aided by the underlying instability being a temporal normal mode which could be equilibrated by second order thermal fluxes (obtained from the second cumulant) modifying the time-independent thermal structure of the mean state (obtained from the first cumulant) to stability by Rayleigh's criterion. The successful application of statistical state dynamics to understanding turbulent convection and anisotropic 2D beta-plane turbulence encouraged a program of applying the statistical state dynamics approach to understand the dynamics of anisotropic 3D wall-bounded turbulence. However, attempts to extend the program of Malkus to obtain the equilibrium state of wall-turbulence as the fixed point of a second order closure of the statistical state dynamics had not succeeded [31]. From the point of view presented in this work the concept of applying the program of Malkus [32] to wall turbulence was essentially correct requiring only the additional recognition that the instability to be equilibrated is the instability of the time-dependent operator associated with linearization about the temporally varying streamwise mean flow. In contrast, the program of Malkus and its variations was predicated on stabilization of the temporal modal instability associated with linearization about a time-independent mean flow. With the additional insight that the instability maintaining the perturbation variance in shear flow turbulence is parametric the equilibrium turbulent state is understood to result from quasi-linear adjustment of the time-dependent mean flow to neutral parametric growth rate of its most unstable structure or structures. The growth rate of these temporally varying structures is given by the maximal Lyapunov exponent of the perturbation covariance equation (this growth rate is necessarily zero given that the turbulence statistics are stationary).

As remarked by Herring [22] second order closures of the statistical state dynamics are necessarily quasi-linear. Model systems that implement a finite ensemble approximation to the statistical state dynamics of the Navier–Stokes equations at second-order are consistently also quasi-linear and we refer to such systems as RNL_N systems (restricted nonlinear systems). The simplest RNL_N system is the RNL_1 system which consists of the streamwise mean equations forced by the Reynolds stresses ob-

tained from the perturbation covariance formed from a single realization of the perturbation dynamics. While the dynamics of the RNL_1 system is formally equivalent to that of a quasi-linear system consisting of a mean flow and a realization of the perturbation dynamics, RNL_N systems for $N > 1$ can only be regarded as approximation to the second order statistical state dynamics. Consistently, we regard our state variables to be the mean flow and the covariance of the perturbations (the first and second cumulants) regardless of how many ensemble members are used to approximate the covariance.

As N increases RNL_N systems approach S3T dynamics, which is a closure of the statistical state dynamics at second order in which an equivalently infinite ensemble is solved for by using a time dependent Lyapunov equation [24]. The S3T system is closed by either setting the third cumulant to zero or by replacing it with a stochastic parameterization. Because S3T dynamics is recovered in the limit $N \to \infty$ we can identify solutions of RNL_∞ systems with S3T. While the use in S3T dynamics of a time-dependent Lyapunov equation to advance the perturbation covariance in time allows direct solution for the second cumulant, corresponding to the covariance obtained from a formally infinite ensemble, the great advantage of RNL_N systems is that although these are approximations to statistical state dynamics they allow extension of second order S3T statistical state dynamics to study turbulence at high Reynolds number [33–35].

The self-sustaining process operating in the S3T system is similar in some ways to previously proposed self-sustaining processes in that a quasi-linear interaction occurs between perturbations and the mean flow to maintain the roll which in turn forces the streak completing the cycle of nonlinear instability [13]. For example, the self-sustaining process of Waleffe [9] and vortex-wave interaction process of Hall & Sherwin and collaborators [10, 36, 37] are also quasi-linear, although this quasi-linearity is imposed by construction rather than resulting from a closure. In the self-sustaining process of Waleffe and that of vortex-wave interaction a single unstable or neutral inflectional mode interacts with the mean flow to transfer energy from the streak to maintain the roll. In contrast, in S3T the streamwise mean flow interacts with a broad spectrum of background turbulence in producing the energy transfer that maintains the roll by a fundamentally non-modal process. Moreover, unlike previously proposed modal instability-based mechanisms or transient growth-based mechanisms [11, 38], the growing perturbations sustaining S3T turbulence result from parametric instability of the time-dependent streak [13]. Parametric instability is generally associated with its application to the study of the stability of a periodically modulated system (cf. Drazin & Reid [39], section 48). We widen application of this term to refer to any linear instability that is inherently caused by the time dependence of the system. The reason we have adopted the same word to describe the instability of periodic and non-periodic flows is that the same non-normality based instability mechanism operates in both cases [40, 41]. Consistent with application of this analysis, nearly all linear time-dependent dynamical systems are destabilized if their fluctuations have sufficiently high amplitude [41]. If the system is not subject to external excitation this instability almost surely manifests asymptotically in time with dominance of the incoherent component of the perturbation dynamics by the structure of the top Lyapunov vector (or vectors in the case of degeneracy) of the associated time dependent linear dynamical operator [40, 42, 43].

In previous work [13, 44] we identified the parametric instability mechanism underlying maintenance of the perturbation variance in S3T Couette turbulence. We also noted its association with the theory of the instability of stochastic time-dependent linear dynamical systems. It follows from this theory that the perturbation dynamics can be decomposed into a basis of Lyapunov vectors (as defined in Appendix A) each characterized by a Lyapunov exponent [42, 43]. This result is analogous to the familiar example of time independent perturbation dynamics in which the dynamics can be decomposed into a basis of eigenvectors each characterized by the exponential growth rate of its associated eigenvalue. This analogy suggests a program of exploiting the known analytical structure of the parametric instability of random time-dependent dynamical systems to gain insight into the dynamics of the incoherent component of the turbulence and particularly the mechanism of the instability that maintains it [40, 41, 45]. Heretofore this incoherent component had been generally thought of as resulting from random transient growth events and scattering by perturbation advection. Characterization of the incoherent component of the turbulence in terms of Lyapunov vectors offers the possibility of understanding these structures more precisely. Moreover, given that a realistic turbulence exists naturally in the S3T self-sustaining state for Couette flow in which only the first Lyapunov vector is supported, the possibility of complete characterization of this, albeit simplified, turbulence becomes available [13, 34, 46]. In this work we isolate the instability mechanism supporting the perturbation structure from the turbulence dynamics by obtaining the time-dependent mean flow from a self-sustaining S3T turbulence and using this time dependent mean flow to force the instability of a completely separate perturbation dynamics that has been randomly initialized. This program is analogous to taking an inflectional streak from an observation of a stationary shear flow and calculating the most unstable temporal normal mode on this streak: one would predict the form of the perturbation structure to be that of the fastest growing mode. In complete analogy we can predict the structure of the turbulent perturbations in this S3T Couette turbulence to be that of the first Lyapunov vector forced by the corresponding time-dependent mean flow. Having obtained the structure of the perturbation component of this simplified turbulence we then proceed to characterize it in terms of its energetics and mechanism of growth. Having obtained complete characterization of this simplified turbulence

supported by only the first Lyapunov vector we then proceed to study the energetics of the remaining Lyapunov vectors which, although damped in this simple model with no parameterized nonlinearity, would be expected to be maintained at finite amplitude by scattering arising from perturbation nonlinearity when a parameterization for nonlinearity is included. The result of implementing such a parameterization for perturbation–perturbation nonlinearity is the prediction that the remaining Lyapunov vectors are robustly supported by direct energetic interaction with the time dependent mean flow. The implication of this result is contrary to the idea that the perturbation variance results from a turbulent cascade or from random transient growth events suggesting rather that spectrally nonlocal interaction with the fluctuating mean flow constitutes a primary mechanism for maintaining the perturbation variance. Furthermore, we show that these analytically characterized Lyapunov vectors together comprise the dominant support for the perturbation variance structure. Having understood the perturbation dynamics in isolation we next proceed to recouple the mean and perturbation systems to recover the complete S3T turbulence dynamics and use this system to study the feedback control mechanism that regulates the turbulence to its statistical steady state.

II. THE S3T STATISTICAL STATE DYNAMICS MODEL

Consider plane Couette flow between walls with velocities $\pm U_w$. The streamwise direction is x, the wall-normal direction is y, and the spanwise direction is z. Lengths are non-dimensionalized by the channel half-width, δ, and velocities by U_w, so that the Reynolds number is $Re = U_w\delta/\nu$, with ν the coefficient of kinematic viscosity. We take for our example a doubly periodic channel of non-dimensional length L_x in the streamwise direction and L_z in the spanwise.

The velocity field is decomposed into a streamwise mean, $\boldsymbol{U}$, with components, (U, V, W), and perturbation from this mean, $\boldsymbol{u}$, with components (u, v, w). The pressure is similarly decomposed into its streamwise mean, P, and perturbation from this mean, p. The non-dimensional Navier-Stokes equations decomposed into an equation for the streamwise mean and an equation for the perturbation are:

$$\partial_t \boldsymbol{U} + \boldsymbol{U}\cdot\boldsymbol{\nabla}\boldsymbol{U} + \boldsymbol{\nabla}P - \Delta\boldsymbol{U}/Re = -\left[\boldsymbol{u}\cdot\boldsymbol{\nabla}\boldsymbol{u}\right]_x \ , \quad \text{(1a)}$$

$$\partial_t \boldsymbol{u} + \boldsymbol{U}\cdot\boldsymbol{\nabla}\boldsymbol{u} + \boldsymbol{u}\cdot\boldsymbol{\nabla}\boldsymbol{U} + \boldsymbol{\nabla}p - \Delta\boldsymbol{u}/Re = -\left(\boldsymbol{u}\cdot\boldsymbol{\nabla}\boldsymbol{u} - \left[\boldsymbol{u}\cdot\boldsymbol{\nabla}\boldsymbol{u}\right]_x\right) + \boldsymbol{f}_e \ , \quad \text{(1b)}$$

$$\boldsymbol{\nabla}\cdot\boldsymbol{U} = 0 \ , \quad \boldsymbol{\nabla}\cdot\boldsymbol{u} = 0 \ , \quad \boldsymbol{\nabla}\cdot\boldsymbol{f}_e = 0 \ , \quad \text{(1c)}$$

where $\boldsymbol{f}_e(x, y, z, t)$ is a stochastic excitation, square brackets denote an average over the variable that appears as subscript, e.g.

$$\left[\,\cdot\,\right]_x \equiv L_x^{-1}\int_0^{L_x} \cdot \, \mathrm{d}x \ , \quad (2)$$

is a streamwise average and $\left[\,\cdot\,\right]_{x,z}$ a streamwise and spanwise average. The velocities and the stochastic excitation $\boldsymbol{f}_e$ satisfy periodic boundary conditions in the z and x directions and no-slip boundary conditions in the cross-stream direction: $\boldsymbol{U}(x, \pm 1, z, t) = (\pm 1, 0, 0)$, $\boldsymbol{u}(x, \pm 1, z, t) = \boldsymbol{f}_e(x, \pm 1, z, t) = 0$. The stochastic excitation is applied only to the streamwise varying Fourier components of the flow, $\left[\boldsymbol{f}_e\right]_x = 0$. The stochastic excitation is nondivergent, has zero ensemble mean, $\langle \boldsymbol{f}_e \rangle = 0$ (angle brackets denote ensemble mean over excitation realizations), is delta correlated in time and statistically homogeneous in x and z. Delta correlation in time implies that the mean energy input by the excitation is independent of the flow state.

The statistical state dynamics of (1) is closed at second order by parameterizing the perturbation–perturbation interactions, $\boldsymbol{u}\cdot\boldsymbol{\nabla}\boldsymbol{u} - \left[\boldsymbol{u}\cdot\boldsymbol{\nabla}\boldsymbol{u}\right]_x$, as a stochastic excitation and associated dissipation. The additional dissipation associated with the stochastic parameterization of the perturbation–perturbation nonlinearity is chosen so that no net energy is introduced by the parameterization as the perturbation–perturbation interactions redistribute energy among the perturbation components without introducing any net energy into the perturbation field. With this parameterization the Navier-Stokes equations are reduced to this quasi-linear equation set, referred to as the restricted nonlinearity (RNL) system:

$$\partial_t \boldsymbol{U} + \boldsymbol{U}\cdot\boldsymbol{\nabla}\boldsymbol{U} + \boldsymbol{\nabla}P - \Delta\boldsymbol{U}/Re = -\left[\boldsymbol{u}\cdot\boldsymbol{\nabla}\boldsymbol{u}\right]_x \ , \quad \text{(3a)}$$

$$\partial_t \boldsymbol{u} + \boldsymbol{U}\cdot\boldsymbol{\nabla}\boldsymbol{u} + \boldsymbol{u}\cdot\boldsymbol{\nabla}\boldsymbol{U} + \boldsymbol{\nabla}p - \Delta\boldsymbol{u}/Re = \boldsymbol{f} - r\boldsymbol{u} \ , \quad \text{(3b)}$$

where $\boldsymbol{f}$ denotes both any external excitation and the parameterization of the perturbation–perturbation interactions. The linear dissipation rate r is chosen so that no net energy is introduced by the part of $\boldsymbol{f}$ that parameterizes the perturbation–perturbation interactions. Both the velocity fields and the excitation satisfy the non-divergence conditions (1c).

It is convenient to use the non-divergence of the mean flow to express the mean dynamics (3a) in terms of the mean streamwise velocity, U, and a mean spanwise/cross-steam velocity streamfunction, Ψ. In these variables (3a) is equivalent to

$$\partial_t U = U_y\Psi_z - U_z\Psi_y - \partial_y\left[uv\right]_x - \partial_z\left[uw\right]_x + \Delta_1 U/Re, \quad \text{(4a)}$$

$$\partial_t \Delta_1\Psi = \left(\partial_y^2 - \partial_z^2\right)\left(\Psi_y\Psi_z - \left[vw\right]_x\right) - \partial_{yz}\left(\Psi_y^2 - \Psi_z^2 + \left[w^2\right]_x - \left[v^2\right]_x\right) + \Delta_1\Delta_1\Psi/Re, \quad \text{(4b)}$$

with $\Delta_1 \equiv \partial_y^2 + \partial_z^2$ and the mean cross-stream and spanwise velocities are given by $V = -\Psi_z$ and $W = \Psi_y$ re-

spectively. Subscripts in flow fields denote differentiation in the variable indicated by the subscript.

Nondivergence of the perturbation velocity field is used to eliminate the pressure from the perturbation equations (3b) by transforming the perturbation dynamics into the variables cross-stream velocity v and cross-stream vorticity, $\eta \equiv u_z - w_x$. In these variables equations (3b), upon neglect of the advection of the perturbations by the smaller magnitude V and W velocities, assume the convenient form:

$$\partial_t \Delta v + U\Delta v_x + U_{zz} v_x + 2U_z v_{xz} - U_{yy} v_x - 2U_z w_{xy} - 2U_{yz} w_x - \Delta\Delta v/Re = f_v - r\Delta v \ , \tag{5a}$$

$$\partial_t \eta + U\eta_x - U_z v_y + U_{yz} v + U_y v_z + U_{zz} w - \Delta\eta/Re = = f_\eta - r\eta \ , \tag{5b}$$

where f_v and f_η are the stochastic excitation in these variables.

We next Fourier expand the perturbation fields and the stochastic excitation fields in x, e.g:

$$v = \Re\left[\sum_{k>0} \hat{v}_k(y,z,t)\, \mathrm{e}^{\mathrm{i}kx}\right] \ ,$$

where $\Re$ denotes the real part, and then write the equations (5) for the evolution of the Fourier components of the perturbations in matrix form:

$$\frac{d\tilde{\phi}_k}{dt} = \tilde{\mathbf{A}}_k(U)\tilde{\phi}_k + \tilde{\mathbf{F}}_k\xi(t) - r\tilde{\phi}_k \ , \tag{6}$$

where the state of the system $\tilde{\phi}_k = [\hat{v}_k, \hat{\eta}_k]^T$ comprises the values of the $\hat{v}_k$ and $\hat{\eta}_k$ on the $N = N_y N_z$ grid points of the (y,z) plane, $\tilde{\mathbf{F}}_k$ is the $2N \times 2N$ matrix determining the spatial structure of the stochastic excitation and ξ is a vector of $2N$ independent zero-mean stochastic processes satisfying:

$$\langle \xi(t_1)\xi(t_2)^\dagger \rangle = \delta(t_1 - t_2)\ \mathbf{I} \ , \tag{7}$$

where $\mathbf{I}$ is the $2N$-identity matrix and $\dagger$ denotes the Hermitian transpose. The matrix $\tilde{\mathbf{A}}_k$ is the discretized coupled Orr–Sommerfeld and Squire operator for perturbations with x-wavenumber k evolving about the instantaneous mean streamwise flow $U(y,z,t)$ [13, 45]. The Fourier amplitudes of the perturbation fields satisfy periodic boundary conditions in x and z and $\hat{v}_k = \partial_y \hat{v}_k = \hat{\eta}_k = 0$ at $y = \pm 1$. The energy density of the perturbations is given by $E = \tilde{\phi}_k^\dagger \mathbf{M}_k \tilde{\phi}_k$, where $\mathbf{M}_k$ is the energy metric. It is convenient to consider the perturbation dynamics (6) transformed to generalized velocity coordinates $\phi_k = \mathbf{M}_k^{1/2}\tilde{\phi}_k$, so that energy is given by the L_2 norm $E = \phi_k^\dagger \phi_k$. The perturbation dynamics in generalized velocity coordinates are governed by:

$$\frac{d\phi_k}{dt} = \mathbf{A}_k(U)\phi_k + \mathbf{F}_k\xi(t) \ , \tag{8}$$

where $\mathbf{A}_k = \mathbf{M}_k^{1/2}\tilde{\mathbf{A}}_k\mathbf{M}_k^{-1/2}$ and $\mathbf{F}_k = \mathbf{M}_k^{1/2}\tilde{\mathbf{F}}_k$.

For an equation with the form (8) the ensemble average perturbation covariance, $\mathbf{C}_k = \langle \phi_k \phi_k^\dagger \rangle$, can be verified to evolve according to the time-dependent Lyapunov equation:

$$\frac{d\mathbf{C}_k}{dt} = \mathbf{A}_k(U)\,\mathbf{C}_k + \mathbf{C}_k\,\mathbf{A}_k^\dagger(U) + \mathbf{Q}_k - r\mathbf{C}_k \ , \tag{9}$$

in which: $\mathbf{Q}_k = \mathbf{F}_k\mathbf{F}_k^\dagger$ [24, 47] and the linear damping is

$$r = \frac{\sum_k \mathrm{Tr}(\mathbf{Q}_k)}{\sum_k \mathrm{Tr}(\mathbf{C}_k)} \ , \tag{10}$$

with $\mathrm{Tr}(\,\cdot\,)$ denoting the trace, $\sum_k \mathrm{Tr}(\mathbf{C}_k)$ the total perturbation energy and $\sum_k \mathrm{Tr}(\mathbf{Q}_k)$ the net energy input rate to all wavenumbers by the stochastic excitation. With this choice for the linear damping the net energy input rate is equal to the perturbation energy dissipation rate at each time instant and no net energy is input to the perturbation field. Parameterizing the third order cumulant in this way is consistent with the requirement that the peturbation–perturbation nonlinearity does not contribute in the net to the perturbation energy. A similar parameterization was previously used to close a statistical state dynamics model of baroclinic turbulence [25]. Finally, we note that under the ergodic assumption that streamwise averages are equal to ensemble averages the Reynolds stress divergences appearing in the streamwise mean equations (4) can be expressed as a linear function of the ensemble average $\mathbf{C}_k$ obtained from the time-dependent Lyapunov equation.

With the parameter choice of our example problem S3T turbulence self-sustains by interaction between the single perturbation structure with wavenumber $k = 2\pi/L_x$ and the mean flow. Perturbations supported by other streamwise wavenumbers that happen to be present in an initial state spontaneously damp out and are not retained in the solution. Further, if stochastic excitation is confined to this supported streamwise wavenumber the subscript k in the velocity and excitation components can be dropped without ambiguity because in the S3T equations the perturbation–perturbation interactions are not included from which it follows that with this choice of excitation the perturbation field has power only in the streamwise component that is forced. The S3T system so restricted self-sustains turbulence in minimal channel Couette flow even at $Re = 400$ [13].

Summarizing, the S3T system we study consists of mean equation (4) coupled with perturbation covariance equation (9):

$$\frac{d\Gamma}{dt} = G(\Gamma) + \mathcal{F}(\mathbf{C}) \ , \tag{11a}$$

$$\frac{d\mathbf{C}}{dt} = \mathbf{A}(U)\,\mathbf{C} + \mathbf{C}\,\mathbf{A}^\dagger(U) + \mathbf{Q} - \frac{\mathrm{Tr}(\mathbf{Q})}{\mathrm{Tr}(\mathbf{C})}\mathbf{C} \ , \tag{11b}$$

where $\Gamma \equiv [U, \Psi]^T$ is the vector of the variables of the

streamwise mean flow, $G(\Gamma)$ expresses the time rate of change of the streamwise mean flow due to self advection and dissipation, while the term $\mathcal{F}(\mathbf{C})$ produces the Reynolds stress forcing of the mean equations from the covariance of the perturbation field, $\mathbf{C}$ (see (4)). For further details on the formulation see Ref. [13].

Results are presented for the minimal Couette flow channel studied by Hamilton, Kim & Waleffe [8] with streamwise length $L_x = 1.75\pi$ and spanwise length $L_z = 1.2\pi$. We use $Re = 600$ (instead of the minimal $Re = 400$ used in Ref. [8]) in order to obtain turbulence statistics without interruption by relaminarization events. For examples in which the retained perturbation streamwise wavenumber, $k = 2\pi/L_x$, is stochastically excited this is done using independent compact support cross-stream velocity and cross-stream vorticity structures in (y, z) chosen to inject equal energy into every degree of freedom in the system. The resulting spatial forcing covariance, $\mathbf{Q}$, is spanwise homogeneous and is consistently taken to be the identity matrix. Numerical calculations employ $N_y = 21$ grid points in the cross-stream direction and $N_z = 30$ grid points in the spanwise direction. A study of S3T turbulence under similar conditions in various channel sizes were reported by Thomas et al. [44].

III. ISOLATING THE LINEAR DYNAMICS OF THE SECOND ORDER CUMULANT

The unforced S3T equations:

$$\frac{\mathrm{d}\Gamma_a}{\mathrm{d}t} = G(\Gamma_a) + \mathcal{F}(\mathbf{C}_a) \ , \tag{12a}$$

$$\frac{\mathrm{d}\mathbf{C}_a}{\mathrm{d}t} = \mathbf{A}(U_a)\,\mathbf{C}_a + \mathbf{C}_a\,\mathbf{A}^\dagger(U_a) \ , \tag{12b}$$

form a non-linear dynamical system that self-sustains S3T turbulence [13, 34, 35, 44, 46]. The quasi-linear structure of this system allows us to isolate the linear dynamics of the incoherent component of the turbulence, $\mathbf{C}_b$:

$$\frac{\mathrm{d}\mathbf{C}_b}{\mathrm{d}t} = \mathbf{A}(U_b)\,\mathbf{C}_b + \mathbf{C}_b\,\mathbf{A}^\dagger(U_b) \ , \tag{13}$$

where $U_b(y, z, t)$ could be an arbitrary time-dependent mean streamwise velocity but for our purposes is taken to be the solution $U_a(y, z, t)$ obtained from a sufficiently long time series of a self-sustaining turbulence solving (12). With U_b chosen to be identical to the fluctuating mean flow, U_a, of the self-sustaining S3T turbulent state, the time dependent linear equation (13) can be verified to have exactly zero Lyapunov exponent and the covariance, $\mathbf{C}_b$, if randomly initialized can be verified to asymptotically approach the rank 1 covariance produced by the structure associated with this zero Lyapunov exponent, which will be referred to as the first Lyapunov vector (cf. Appendix A). From the theory of time-dependent linear dynamical systems we know that as $t \to \infty$ the covariance can be decomposed into a basis of time dependent Lyapunov vectors ordered in average growth rate by their Lyapunov exponents [42, 43, 48]. This result obtained in the case of a time dependent linear dynamics is analogous to the more familiar case of a time independent linear dynamics in which as $t \to \infty$ the analogous covariance can be decomposed into a basis of orthogonal time independent vectors which, with the exception of the first, are not identical to the eigenvectors of the associated time independent dynamical operator but are ordered in growth rate by the associated dynamical operator's eigenmode growth rates. In both the autonomous and non-autonomous case the covariance is exponentially dominated by the most unstable of these which has the structure of the most unstable Lyapunov vector and eigenmode respectively.

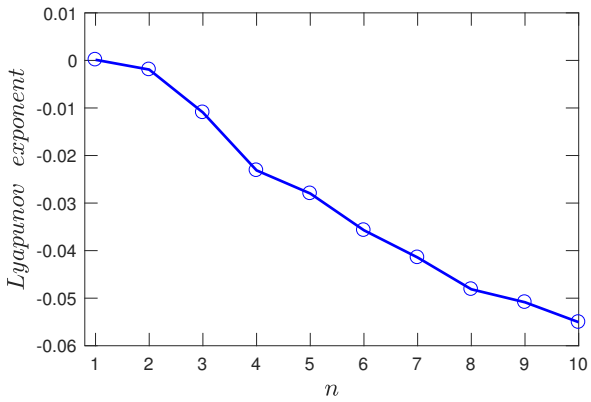

FIG. 1: The first ten Lyapunov exponents of the dynamical operator $\mathbf{A}(U_a)$. The maximal Lyapunov exponent is zero, consistent with U_a being the consistent time dependent mean streamwise component supporting the turbulent perturbation component of the combined turbulent state.

Consider forcing the secondary perturbation dynamics (13) to have the same time dependence as the primary self-sustaining S3T turbulent system (12) by setting $U_b = U_a$ in (13). The first question we address is whether this coupling results in synchronization of the perturbation fields. Under forcing by U,the first 10 Lyapunov exponents of a randomly initialized $\mathbf{C}_b$, are shown in Fig. 1. The maximal Lyapunov exponent of $\mathbf{C}_b$ assumes the same zero value as that of $\mathbf{C}_a$ and both $\mathbf{C}_a$ and $\mathbf{C}_b$ assume asymptotically the structure associated with the same corresponding first Lyapunov vector. However, $\mathbf{C}_a$ and $\mathbf{C}_b$ differ in amplitude (to the degree the random initial state of $\mathbf{C}_b$ projects on the first Lyapunov vector). Therefore it is required to use as a synchronization condition convergence of the normalized covariances:

$$\lim_{t\to\infty} \delta(t) \equiv \lim_{t\to\infty} \left\| \frac{\mathbf{C}_a}{\|\mathbf{C}_a\|} - \frac{\mathbf{C}_b}{\|\mathbf{C}_b\|} \right\| = 0 \ . \tag{14}$$

Convergence in this measure proceeds on average at twice the rate of the decaying second Lyapunov exponent

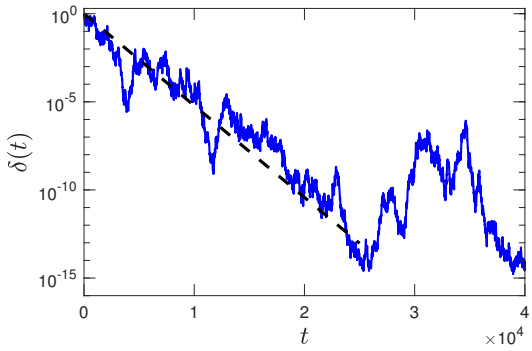

FIG. 2: The approach towards synchronization measured by $\delta(t)$ occurs at twice the rate of the second Lyapunov exponent of $\mathbf{A}(U_a)$, which is indicated with the dashed line.

of $\mathbf{A}(U_a)$, as shown in Fig. 2. To within streamwise phase the first Lyapunov vector of the primary system, which is the top singular vector of $\mathbf{C}_a$, is identical to the first Lyapunov vector of the secondary system, which is the top singular vector of $\mathbf{C}_b$, as shown in Fig. 3.

While both $\mathbf{C}_a$ and $\mathbf{C}_b$ are with exponential accuracy rank one, as they are both the covariance produced by the first Lyapunov vector, eigenanalysis of either $\mathbf{C}_a$ or $\mathbf{C}_b$ reveals the remaining Lyapunov vectors of the linear time dependent system (13) which are decaying with time at the rate of their Lyapunov exponents as shown in Fig. 1. This decay of the Lyapunov vectors in the order of their (negative) Lyapunov exponents is shown in Fig. 4. We remark that support of the turbulence by the single top Lyapunov vector is obtained when scattering by the perturbation–perturbation nonlinearity is ignored ($\mathbf{Q} = 0$ in (11)). This turbulence provides an opportunity to study the physical mechanisms of self-sustaining turbulence in maximally simplified form. We will relax the assumption $\mathbf{Q} = 0$ after our initial study of this maximally simplified self-sustaining state in order to study the effect of perturbation–perturbation nonlinearity on the turbulence and specifically the role played by the remaining Lyapunov vectors when these are maintained by excitation parameterizing scattering of energy by the perturbation–perturbation nonlinearity.

We have verified that the incoherent perturbation structure in S3T turbulence can be analytically identified with the first Lyapunov vector of the time dependent perturbation operator, $\mathbf{A}(U)$, linearized about the instantaneous streamwise mean flow $U(y, z, t)$. This perturbation structure has zero Lyapunov exponent and in that sense it is the neutral structure corresponding to the time dependent streamise mean velocity.

IV. ENERGETICS OF THE LYAPUNOV STRUCTURES UNDERLYING THE INCOHERENT COMPONENT OF S3T TURBULENCE

Having determined the analytical structure of the perturbation field to be that of the top Lyapunov vector of the fluctuating perturbation dynamics we consider next the mechanism maintaining this structure. We will show that the perturbation component of the turbulence is not maintained by temporal mode instability but rather by parametric instability. Parametrically unstable systems are unstable due to the interaction between the non-normality and the time dependence of the dynamical operator rather than to temporal mode instability of the operator at individual instants of time. In fact, instability of the operator is irrelevant to parametric instability as the familiar analysis of parametric instability in the damped pendulum using the Mathieu equation demonstrates.

In order to study this parametric instability mechanism in detail the following analysis is performed: at each instant the normalized perturbation state, ϕ, is projected on the ellipsoid the principal axes of which are in the directions of the eigenvectors of the symmetric matrix $\mathbf{A}+\mathbf{A}^\dagger$. By eigen-decomposition $\mathbf{USU}^\dagger = \mathbf{A}+\mathbf{A}^\dagger$ with $\mathbf{U}$ the matrix composed of the instantaneous eigenvectors of $\mathbf{A}+\mathbf{A}^\dagger$ arranged in columns and $\mathbf{S}$ the diagonal matrix of the corresponding eigenvalues. The instantaneous growth rate of perturbation energy is given by

$$g(t) = \frac{\phi^\dagger \mathbf{USU}^\dagger \phi}{\phi^\dagger \phi} \ . \tag{15}$$

Similarly, we can calculate the growth rate of the perturbation energy that would be obtained if the eigenmodes were orthogonal with their same eigenvalues by forming the ellipsoid the principal axes of which correspond to the instantaneous growth rate of the eigenmodes of $\mathbf{A}$ and projecting the normalized state on these eigenmodes. The normalized projections of the perturbation state ϕ on this ellipsoid are then the instantaneous equivalent normal growth rates i.e. the growth rates that would occur if $\mathbf{A}$ were a normal matrix with these eigenvalues. The equivalent normal energy growth rate is given by

$$h(t) = \frac{\phi^\dagger \mathbf{EDE}^{-1} \phi}{\phi^\dagger \mathbf{E}^{-1\dagger} \mathbf{E}^{-1} \phi} \ , \tag{16}$$

where $\mathbf{E}$ is the matrix consisting of the instantaneous eigenvectors of $\mathbf{A}$ arranged in columns and $\mathbf{D}$ is the diagonal matrix of twice the associated modal growth rates of the modes.

The probability density function of the eigenvalues of $\mathbf{A}+\mathbf{A}^\dagger$, which correspond to the axes of the instantaneous growth rate ellipsoid, and the probability density function of twice the real part of the eigenvalues of $\mathbf{A}$, which correspond to the axes of the modal growth rate ellipsoid, are shown for a self-sustaining turbulent state in the

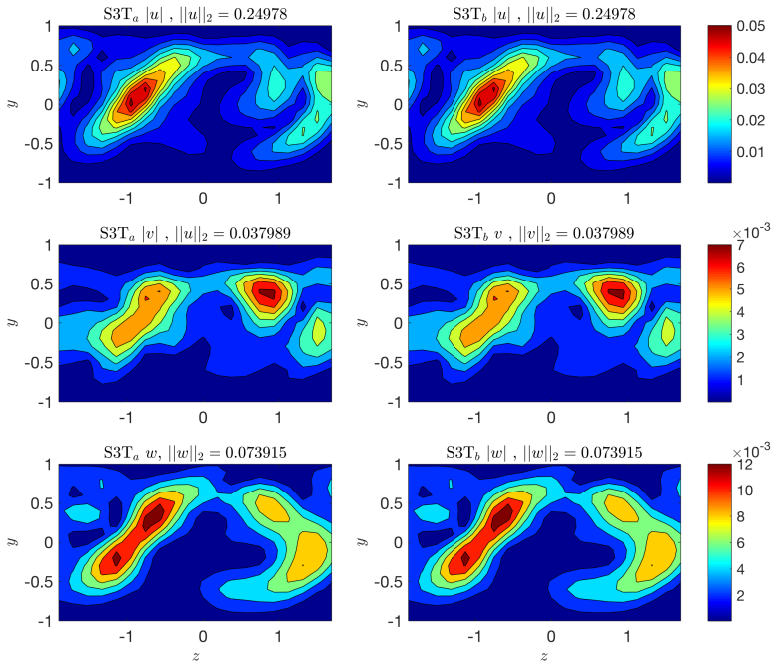

FIG. 3: The three components of perturbation velocity, u,v, and w (in sequence from top to bottom) of the first Lyapunov vector (LV_1), which is the eigenvector with the largest eigenvalue of the covariance $\mathbf{C}_a$ of the primary system (left panels) and similarly for the secondary system with covariance $\mathbf{C}_b$ (right panels) initialized with a different initial condition. The snapshots are at $t = 3 \times 10^4$, which is a sufficient time for the asymptotic state to be obtained. The figure demonstrates that in this S3T turbulent state the time varying mean streamwise streak velocity results asymptotically in a unique (to within a streamwise phase) perturbation state to which initial conditions converge. The normalized velocities are represented by contours of their absolute magnitude.

example system over a time interval $\tau = 5000$ in Fig. 5. The instantaneous growth rate of the perturbation state is determined by its projection on the instantaneous growth rate ellipsoid. This projection varies in time due to both the time dependence of the state vector and the time dependence of the growth rate ellipsoid. The distributions of the resulting projections for a turbulent simulation over a time period $\tau = 5000$ is shown in Fig. 6. This figure contains information on both the extent of the growth rates sampled by the state vector as well as the frequency with which these values are sampled. The state vector fails to explore the extremities of the growth rate ellipsoid with most projections being confined around zero growth rate. The information in Fig. 6 is summarized by the cumulative distribution function of the square projections of the state on the principal axes of the growth rate ellipsoid shown in Fig. 7. This cumulative distribution function is obtained from Fig. 6 by forming

$$F(\sigma) = \frac{\int_{-\infty}^{\sigma} \delta(\sigma' - \sigma_i)|\alpha_i|^2 \, \mathrm{d}\sigma'}{\int_{-\infty}^{\infty} \delta(\sigma' - \sigma_i)|\alpha_i|^2 \, \mathrm{d}\sigma'} \ , \tag{17}$$

in which each of the points in Fig. 6 is a sample $(\sigma_i, |\alpha_i|^2)$. The smooth derivative of the cumulative distribution function, $f(\sigma) = dF(\sigma)/d\sigma$, also shown in Fig. 7, is the probability density function of the perturbation state projections, $|\alpha(\sigma)|^2$, on the energy growth rate, σ. Despite the wide distribution of available growth rates (cf. Fig. 5) the self-sustained state projects on growth rates narrowly centered around zero with values primarily in the interval $[-1, 1]$. The mean growth rate of the state,

$$\lambda = \int_{-\infty}^{\infty} \sigma f(\sigma) \, \mathrm{d}\sigma \ , \tag{18}$$

vanishes consistent with the perturbation being a component of the statistically stable turbulent state trajectory, i.e. the state trajectory, corresponding to the first Lyapunov vector (LV_1), has been adjusted, together with and by mutual interaction with the mean flow, to have zero Lyapunov exponent. An equivalent diagnostic, the growth rate probability density function, is more easily obtained directly from the time series of the growth rates of the individual Lyapunov vectors (LV's). This probability density function is shown for LV_1, and also for the decaying second, third and tenth Lyapunov vectors, LV_2, LV_3, and LV_{10}, in Fig. 8 in which it can be seen that, although the probability density function of LV_1 peaks at positive growth rates it has a small negative skew and

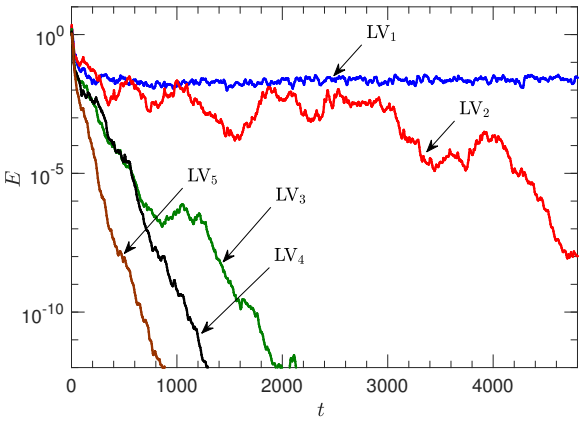

FIG. 4: Evolution of the energy of the first 5 Lyapunov vectors (LV) of the perturbation covariance dynamics which has been synchronized with the mean flow of the turbulent S3T system (12a) and initialized white in energy. The streamwise wavenumber of all the Lyapunov vectors is $k = 2\pi/L_x$ so the individual members of the orthogonal set of Lyapunov vectors differ only in their $y-z$ structure. The maximal Lyapunov exponent associated with the first Lyapunov vector (LV_1) is zero consistent with it constituting a component of the statistical steady state. Except for LV_1, the remaining Lyapunov vectors (LV's) decay at the rate of their negative Lyapunov exponents. However, the second Lyapunov vector (LV_2) has a small negative Lyapunov exponent and exhibits large excursions associated with the time dependence of the dynamical operator.

its mean growth rate is zero and although LV_2 has a negative Lyapunov exponent, it is similar to LV_1 in its energetics. Energetics of the Lyapunov vectors can be more closely analyzed by separating the operator of the linear perturbation dynamics into dynamical and dissipation components by partitioning it as

$$\mathbf{A}(U) \equiv \mathcal{A}(U) + \mathcal{D} \ . \tag{19}$$

In (19) $\mathcal{A}(U)$ is the part of the matrix $\mathbf{A}(U)$ that depends on U and its spatial derivatives and represents dynamic interaction of the perturbation field with the streamwise mean flow, including the transfer of energy between mean and perturbations, and $\mathcal{D}$ is the part of the matrix $\mathbf{A}$ associated with viscous damping. The terms involved in this separation can be identified in the pre-transformed perturbation equations (5). With this splitting the rate of transfer of mean flow energy to a given perturbation, $g_{\mathcal{A}}$, is given by the normalized projection of that perturbation on the Hermitian matrix $\mathcal{A} + \mathcal{A}^\dagger$. Similarly, the rate of dissipation, $g_{\mathcal{D}}$, is given by its normalized projection on $\mathcal{D}^\dagger + \mathcal{D}$. The probability density function of $g_{\mathcal{A}}$ for a selection of Lyapunov vectors and the probability density function of the corresponding decay rates due to dissipation, $g_{\mathcal{D}}$, shown in Fig. 9, reveals that the asymptotic decay of Lyapunov vectors of order 2 and higher is due to enhanced dissipation rather than to inability to gain energy from the mean flow. In fact, mean flow energy is transferred to LV2 at a greater rate than it is to LV1 as seen in Fig. 9. In Fig. 10 is shown the time-mean growth rate of these Lyapunov vectors due to energy transfer from the mean flow, $\overline{g_{\mathcal{A}}}$, and the corresponding magnitude of their mean energy decay rate due to dissipation, $|\overline{g_{\mathcal{D}}}|$ (overbar denotes time average). These average growth and decay rates determine the Lyapunov exponent of the corresponding Lyapunov vector, which is given by $\overline{g_{\mathcal{A}}} - |\overline{g_{\mathcal{D}}}|$. It is interesting to note that although all Lyapunov vectors, except LV_1, are decaying, exactly half of the Lyapunov vectors receive energy from the mean. This property is a corollary of the "time-reversal symmetry" of the inviscid perturbation dynamics that is governed by $\mathcal{A}$. This symmetry of inviscid dynamics is the expression of the invariance of the perturbation evolution equations (5) (in the absence of dissipation or excitation) to the transformation $t \to -t$ and $x \to -x$. This symmetry implies that if $\phi(x,t)$ is a solution of the inviscid equations (5) without excitation, by necessity $\phi(-x,-t)$ is also a solution of (5) and hence if $\phi(x,t)$ grows at the rate λ, $\phi(-x,-t)$ grows at the same rate and by reversing time, $\phi(-x,t)$ decays at rate $-\lambda$. This implies that if ϕ is a Lyapunov vector of $\mathcal{A}(U)$ with Lyapunov exponent λ then ϕ^* is also a Lyapunov vector with Lyapunov exponent $-\lambda$. The fact that fully half the perturbation structures extract energy from the fluctuating mean flow has important consequences for the maintenance of perturbation variance in turbulence as it implies a mechanism for direct non-local in scale transfer of energy from the externally forced large scale mean flow to the small scale perturbation components of the turbulence. This fact invites the conjecture that the mechanism maintaining the incoherent component of perturbation energy in S3T turbulence when parameterization of the third cumulant is restored in the S3T dynamics is parametric interaction with the mean flow and that the structure of the turbulent perturbations is primarily determined by the structure of the LV's. We will restore stochastic parameterization of the third cumulant to examine this conjecture further in the next section.

Another implication of the parametric dynamics maintaining the incoherent perturbation component is that the decaying Lyapunov vectors undergo large excursions in energy (cf. Fig. 4). Such large excursions are characteristic of the energetics of stochastic dynamical systems with multiplicative noise [41, 49, 50]. When a parameterization for the excitation of Lyapunov vectors by perturbation–perturbation nonlinearity is included we expect that a broad spectrum of incoherent perturbations will be supported by interaction with the mean flow. Moreover, these structures undergo large excursions and these excursions have important implications for the dynamics of S3T turbulence. We will further explore these matters but first we wish to examine the dynamics of the parametric mechanism in more detail.

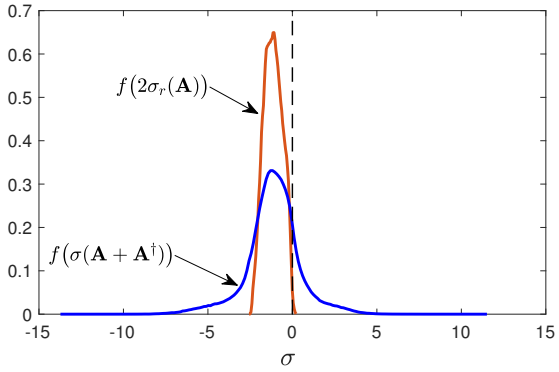

FIG. 5: The probability density function of the eigenvalues of the instantaneous perturbation operators $\mathbf{A}+\mathbf{A}^\dagger$ and of twice the real part of the instantaneous eigenvalues of $\mathbf{A}$ for mean states that occur over a time period $\tau = 5000$. The mean growth rate for both cases is -1.14 (as the real part of the trace of $\mathbf{A}$ is equal to the trace of $(\mathbf{A}+\mathbf{A}^\dagger)/2$), the standard deviation of $\sigma(\mathbf{A}+\mathbf{A}^\dagger)$ is 1.6 and the range in the specific simulations is $[-18.2, 16.2]$, while the standard deviation of $2\sigma_r(\mathbf{A})$ is 0.5 and the range is $[-2.9, 0.4]$. The eigenvalues of $\mathbf{A}+\mathbf{A}^\dagger$ correspond to the axes of the energy growth rate ellipsoid. The extrema of these possible growth rates exceed that of the instantaneous energy eigenfunction growth rates as expected for a non-normal system. Remarkably, only very small positive modal growth rates occur suggesting that the system is constrained to limit the extent of modal instability.

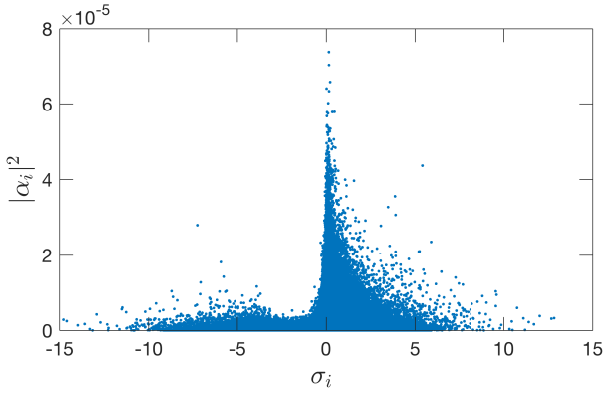

FIG. 6: Instantaneous projections of the normalized state vector on the axes of the ellipsoid of energy growth rate. Each point has coordinates $(\sigma_i, |\alpha_i|^2)$ where σ_i is the i-th eigenvalue of $\mathbf{A}+\mathbf{A}^\dagger$ and $|\alpha_i|^2$ is the square amplitude of the projection of the normalized state on this principal axis. This figure reveals both the magnitude of the projection of the state on the growth rate axes and, by the density of the points, the frequency of the occurrence of each growth rate.

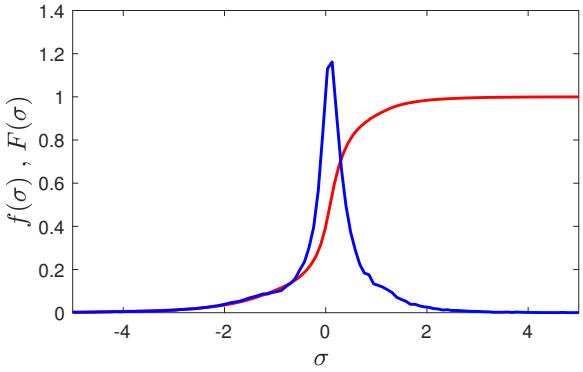

FIG. 7: Cumulative distribution function, $F(\sigma)$, of the square projection of the normalized perturbation state consisting of the first Lyapunov vector on the axes of the growth rate ellipsoid (red). The smooth derivative of the cumulative distribution function, $f(\sigma)$, (shown in blue), is the probability density function of the perturbation state projections $|\alpha(\sigma)|^2$ on the energy growth rate ellipsoid.

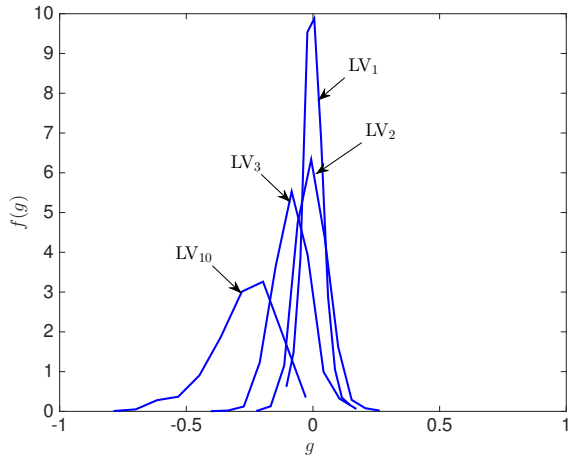

FIG. 8: The probability density function of the instantaneous energy growth rates of Lyapunov vectors LV_1, LV_2, LV_3 and LV_{10}. The second in growth rate Lyapunov vector, LV_2, is only slightly decaying and has a narrowly confined distribution similar to that of the first Lyapunov vector, LV_1, while the LV_3 and LV_{10} decay strongly and sample a wider range of growth rates.

The linear perturbation dynamics is strongly time dependent with the dynamical operator $\mathbf{A}$ and associated growth rate ellipsoid being modified continuously in time by fluctuations in the mean streamwise velocity. These fluctuations cause the dynamics of the interaction between the mean flow and the perturbation field to exhibit large excursions in growth rate on short time scales. In contrast, as shown in Fig. 5, the system adjusts to support only weak instantaneous inflectional instability. A time series of the maximum instantaneous modal growth

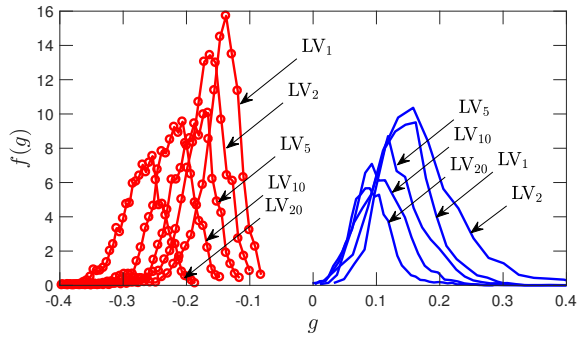

FIG. 9: Partition of the probability density function of the instantaneous energy growth rates of Lyapunov vectors LV_1, LV_2, LV_5, LV_{10} and LV_{20} arising from energy transfer to these vectors from interaction with the streamwise mean flow (curves on the right) and dissipation (curves on the left). The probability density function of the instantaneous growth rates of each Lyapunov vector, shown in Fig. 8, is the sum of these contributions for each LV. A substantial number of higher order Lyapunov vectors robustly extract energy from the mean. In fact, half the LV's extract some energy directly from the mean flow.

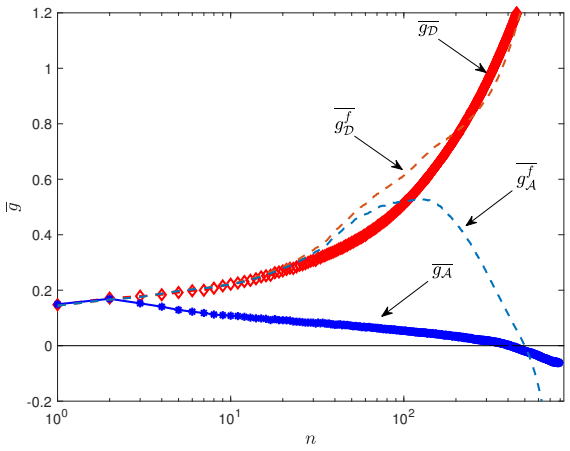

FIG. 10: Mean contribution to the energy growth rate of the Lyapunov vectors due to energy transfer from the mean flow, $\overline{g_{\mathcal{A}}}$ as a function of Lyapunov vector index. Also shown is the magnitude of the mean decay rate of the Lyapunov vectors due to diffusion, $|\overline{g_{\mathcal{D}}}|$. The Lyapunov exponent of each Lyapunov vector is the difference between these two curves. The dashed curve, $\overline{g^f_{\mathcal{A}}}$, shows the average energy transfer rate from the mean to each of the orthogonal eigenfunctions of the covariance $\mathbf{C}$ under external excitation (the SFLV's of the stochastically maintained perturbation field) and the dashed curve, $|\overline{g^f_{\mathcal{D}}}|$, the average decay rate of each of the SFLV's. This figure shows that a substantial subset of SFLV's have neutral energetics and therefore are maintained at finite amplitude by transfer of energy from the mean flow induced by the energy neutral parameterization of perturbation–perturbation nonlinearity (the asymptotic rank of $\mathbf{C}$ is about 50).

rate, σ_r, is shown in Fig. 11. The mean of the maximum growth rate is only 0.045 and the growth rate varies rapidly. Also shown is the time series of the normalized fluctuations of the maximum streak amplitude $U_s^m \equiv \max(U_s(y,z)) - \min(U_s(y,z))$ together with normalized fluctuations of the maximum growth rate, $\sigma_r' = \sigma_r - \langle\sigma_r\rangle$. The streak amplitude and the maximum instability growth rate are substantially correlated consistent with inflectional instability of the streak. However, while the state dynamics adjusts to consistently exhibit a small and rapidly varying instantaneous modal instability, this instability is not itself responsible for sustaining the perturbation variance. Shown in Fig. 12 is the autocorrelation and crosscorrelation of streak amplitude and maximum modal growth rate. The streak and modal instability are correlated with essentially zero lag, as expected for inflectional mode instability, but both of these quantities decorrelate in approximately ten time units which is inconsistent with emergence of the modal instability which has an approximate e-fold time of 20 (cf. Fig. 11). That modal growth does not account for maintenance of the perturbation variance is confirmed in Fig. 13 in which is shown a time series of the energy growth rate of the perturbation field together with the energy growth rate that would occur if the state were projected on the eigenvectors of the instantaneous operator, $\mathbf{A}$, with each advanced at the rate of the corresponding real part of the eigenvalue of $\mathbf{A}$. Although it can be seen from Fig. 11 that the instantaneous mean flow is nearly always weakly modally unstable, it can be seen from Fig. 13 that the contribution to maintaining the Lyapunov vector of the perturbation trajectory arising from modal growth is almost always negative with the time mean value of this equivalent normal contribution to the energy of the perturbation field being decay at rate -0.7. In contrast, the non-normal parametric mechanism produces robust excursions of both positive and negative growth rate due to rapidly varying projections of the perturbation state on the also rapidly varying directions of growth associated with variation of the streak (cf. Fig. 12). Because the maximum Lyapunov exponent is zero and equal to the time integral of the instantaneous growth rates, these positive and negative contributions average of necessity to zero. The Lyapunov exponent is zero as the associated Lyapunov vector is being adjusted through interaction with the streak to be a component of the system's statistically stable trajectory (cf. Fig. 13). Parametric growth is a general attribute of dynamical systems with stochastically fluctuating dynamical operators which are of necessity non-normal with measure zero exception. This statistically sustained growth arises from the concatenation of non-normal growth events which

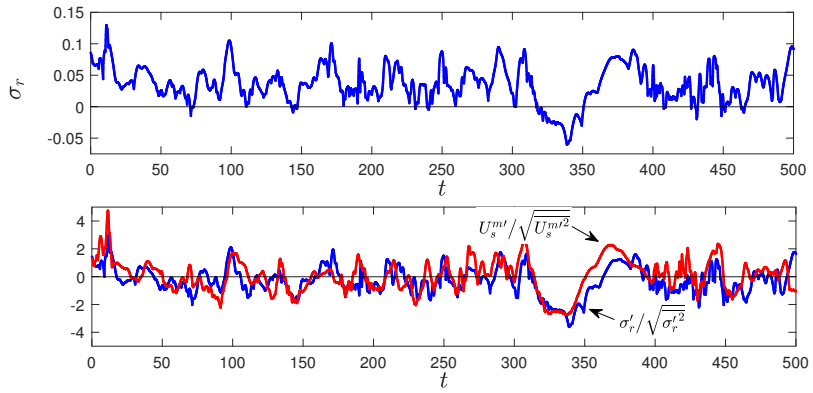

FIG. 11: Panel (a): The maximum modal growth rate of $\mathbf{A}(U)$ over a typical interval in the example system. The mean of the maximum growth rate over the entire time series is 0.045 and the range is $[-0.06, 0.135]$. Panel (b): Corresponding time series of the normalized fluctuations of the maximum growth rate, $\sigma_r' = \sigma_r - \overline{\sigma_r}$, and of the normalized fluctuations of the maximum streak amplitude $U_s^m \equiv \max(U_s(y,z)) - \min(U_s(y,z))$. The streak amplitude and the maximum instability growth rate are correlated with correlation coefficient $r = 0.4$ consistent with inflectional instability of the streak. However, while the state is tightly constrained to exhibit small but consistent instantaneous modal instability, this instability is not responsible for sustaining the perturbation variance.

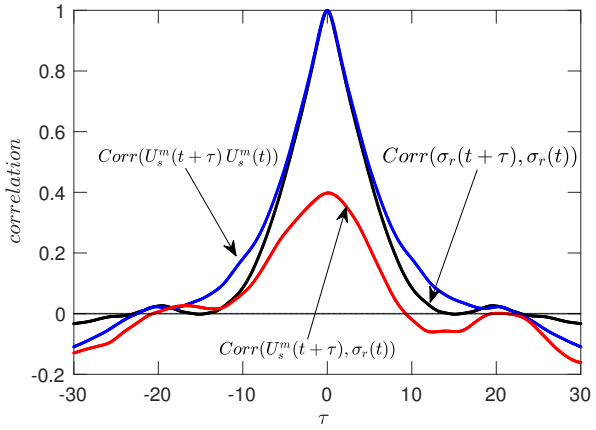

FIG. 12: Autocorrelation of streak amplitude, $U_s^m \equiv \max(U_s(y,z)) - \min(U_s(y,z))$, and maximum modal growth rate, σ_r. Also shown is the cross correlation of these quantities. The streak and modal instability are highly correlated as expected for inflectional mode instability but both of these quantities decorrelate in approximately ten time units which is too short a time for the modal instability to emerge given its typical time scale for growth of approximately 20 time units (cf. Fig. 11).

dominate over decay events due to the convexity of the exponential propagator of the dynamics over the time scale of the operator fluctuation [40, 41]. A characteristic property of stochastic parametric growth is the requirement for the parametric variation of the system to occur on intermediate time scales. This is because the convexity of the exponential vanishes at short dynamical operator fluctuation time scales and the transient perturbation growth vanishes at long time scales. Fluctuations of the streak and the fluctuation in the growth rate of LV_1 fit a red noise process as shown in Fig. 14. Consistent with the stochastic parametric growth mechanism, the correlation time of this red noise process, $\tau = 5.0$, occurs on an intermediate time scale. Moreover, this time scale is short compared to the modal growth time scale so that asymptotic modal growth is not relevant (cf. Fig. 11).

V. DYNAMICS OF THE DECAYING LYAPUNOV STRUCTURES IN THE PRESENCE OF PARAMETERIZED NONLINEAR EXCITATION

Consider S3T dynamics (11) under stochastic excitation with covariance $\mathbf{Q}$ and linear dissipation at the variable rate $\mathrm{Tr}(\mathbf{Q})/\mathrm{Tr}(\mathbf{C})$. This dissipation rate is chosen so that the energy input rate $\mathrm{Tr}(\mathbf{Q})$ is equal to the dissipation rate at each time instant so that no net energy is injected into the perturbation field, consistent with the property that the third-order cumulant being parameterized does not contribute in the net to the perturbation energy. It is an interesting attribute of even time-independent non-normal dynamical systems that although this excitation inputs no net energy to the perturbations, still a non-vanishing pe

rturbation field can be sustained by it. This is in contrast to normal system dynamics, for in that case the perturbation energy evolution equation, which is the trace of (11b), obeys:

$$\frac{d\mathrm{Tr}(\mathbf{C})}{dt} = \mathrm{Tr}\left((\mathbf{A}+\mathbf{A}^\dagger)\mathbf{C}\right) \ , \qquad (20)$$

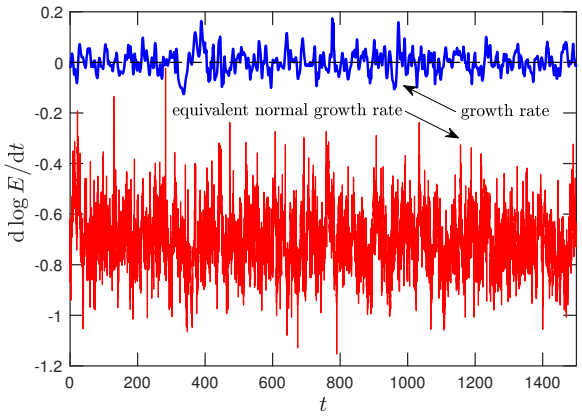

FIG. 13: Time series of the energy growth rate of the perturbation field (blue). This growth rate is equal to the projection of the normalized state on $\mathbf{A}+\mathbf{A}^\dagger$ and its mean value is the Lyapunov exponent of LV_1, which is zero. Energy growth rate that would occur if the state were projected on the eigenvectors of instantaneous operator $\mathbf{A}$ and each advanced at the rate of the corresponding real part of the eigenvalue of $\mathbf{A}$ is also shown (red). The mean value of this equivalent normal growth rate is -0.7. We conclude that while the instantaneous mean states are often modally unstable (cf. Fig. 11) the perturbation state does not project sufficiently on the instabilities to account for its growth. This result demonstrates that the perturbation field is sustained by the parametric non-normal growth process rather than by modal instability.

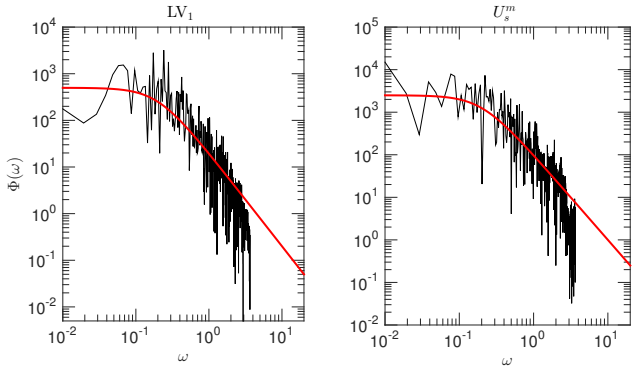

FIG. 14: Spectral density of the energy growth rate of the first Lyapunov vector (LV_1) and of the maximum streak velocity time series and their fit to the Lorentzian $625\tau^{-2}/((\omega\tau)^2+1)$ and $100U_s^m\tau^2/((\omega\tau)^2+1)$ with $\tau=5.0$, respectively. This graph shows that the instantaneous growth rate of the perturbations are well approximated by a red noise process and that the streak fluctuations follow the same red noise process.

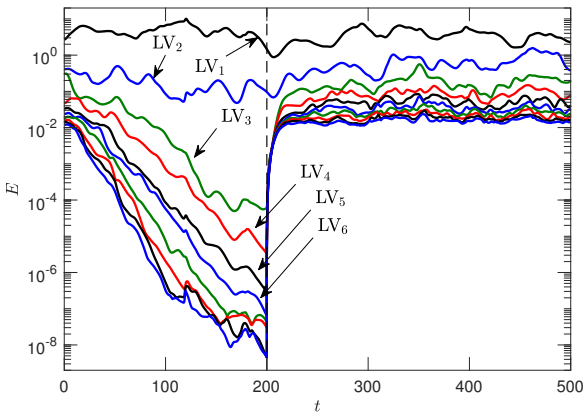

FIG. 15: Evolution of the energy of the first 10 eigenfunctions of the covariance $\mathbf{C}$ with the highest energy. For $t<200$ the covariance dynamics evolves without stochastic excitation and the structures shown are the first 10 Lyapunov vectors of $\mathbf{A}(U)$, of which only LV_1 would be sustained while the other Lyapunov vectors (even LV_2) would decay to zero. A stochastic excitation that imparts no mean energy to the perturbations is introduced at $t=200$. Despite the zero energy input by this parameterization, the non-normality of the time dependent $\mathbf{A}(U)$ sustains a perturbation covariance of rank approximately 50 supported by structures close to the corresponding Lyapunov vectors as shown in Fig. 16.

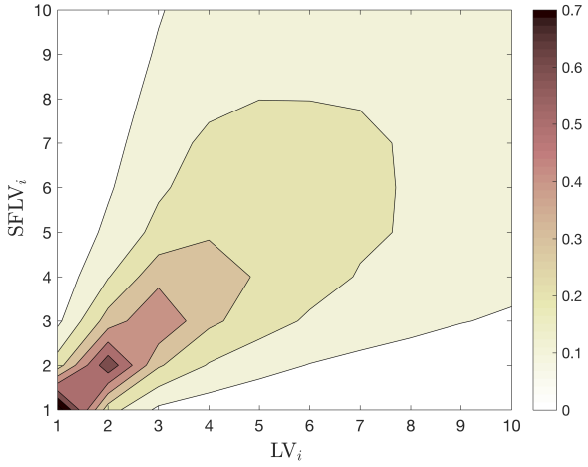

FIG. 16: Contour plot of the average absolute value of the inner product, $|\mathrm{SFLV}_i^\dagger\,\mathrm{LV}_j|$ with $i,j=1,\ldots,10$, between the top 10 SFLV's (the normalized eigenvectors of the $\mathbf{C}$ under stochastic excitations) and the first 10 LV's of $\mathbf{A}(U)$ with the same streamwise mean flow, U. This figure shows that the SFLV's with substantial energy are correlated in structure with the top LV's. The level of excitation is such that if it were imposed on the time mean flow it would support perturbation energy 1% of the mean energy of the unperturbed Couette flow.

which implies that Tr(**C**) will asymptotically vanish if **A** is normal and has decaying modes. Such a forcing can sustain a non-vanishing covariance of substantial rank when **A** is non-normal even should all modes of the system be damped. That a high-rank perturbation covariances can be sustained in a turbulent system with a stochastic parameterization of the third cumulant characterized by zero energy injection has been previously demonstrated in the context of a discussion of the statistical state dynamics of two-layer baroclinic turbulence [25]. A turbulent state with high rank **C** is also maintained in the S3T turbulence of our Couette flow with an energy neutral parameterization of the third order cumulant, as shown in Fig. 15. In this simulation we have initialized the S3T dynamics with a full rank **C**. The stochastic excitation parameterization of the third cumulant which injects no energy is introduced at $t = 200$. In the absence of excitation the covariance is seen to be in the process of collapsing to the rank 1 covariance of the first Lyapunov vector with the remaining Lyapunov vectors decaying at the rate of their respective Lyapunov exponents. When the excitation is imposed the covariance rapidly adjusts to maintain a statistically steady state with finite rank (in this example the rank is approximately 50). The eigenvectors of the finite rank perturbation covariance which are maintained by energy transfer from the fluctuating mean (as shown in Fig. 10) are called, in analogy to the unforced case, the stochastically forced Lyapunov vectors (SFLV). These SFLV's inherit the structure of their associated Lyapunov vectors (LV's) as can be seen from Fig. 16 in which the energy norm projections of the LV's and SFLV's are shown as a contour plot. Diagonal dominance in this plot indicates that the stochastically maintained Lyapunov vectors are correlated in structure with the underlying Lyapunov vectors which decay in the absence of excitation.

VI. MECHANISM REGULATING THE STATISTICAL MEAN STATE OF S3T TURBULENCE

We turn next to study of the mechanism by which the state of S3T turbulence is regulated to its observed statistical mean. The observation that the streak is constrained to be marginally unstable (cf. Fig. 5 and Fig. 11) suggests that the regulation of the turbulent state may be associated with adjustment to marginal streak stability [13]. To study the dynamical mechanism regulating the turbulence to a statistical steady state we make use of an analysis of the energetics of the streak (cf. Appendix. B).

In Fig. 17a is shown a time series of the Reynolds stress and lift-up terms that contribute to the maintenance of the streak energy. Of note is that the Reynolds stress term in the streak energy equation is always negative. In Fig. 17b is shown the autocorrelation of the streak energy ϵ_s, of the perturbation Reynolds stress divergence term in the streak energy equation, $\dot{\epsilon}_F$, of the contribution of the lift-up in the acceleration of the streak, $\dot{\epsilon}_L$, together with the cross correlation of $\dot{\epsilon}_F$ with ϵ_s and of $\dot{\epsilon}_L$ with ϵ_s. The correlation between time series $f(t)$ and $g(t)$ is defined as

$$Corr(f,g) \equiv \frac{\overline{(f-\overline{f})(g-\overline{g})}}{\sqrt{\overline{(f-\overline{f})^2}\;\overline{(g-\overline{g})^2}}} \; . \tag{21}$$

The cross correlation between ϵ_s and $-\dot{\epsilon}_F$ reveals that these quantities are correlated with a $\tau = 5$ lead of the streak energy over the Reynolds stress term. This correlation with short lead time in which streak energy maxima are followed by strong Reynolds stress damping indicates a rapidly acting regulation of the streak energy by the Reynolds stress. The small lead time indicates that transient growth on the advective time scale rather than instability growth on the much longer instability time scale ($1/\sigma_{\max} \approx 20$) is involved in this regulation of the streak energy (cf. Fig. 11). Note the symmetrical behavior of the lift-up acceleration which leads the streak by 5 units of time.

The availability of very rapidly growing fluxes that damp streak energy and that are strongly correlated with streak amplitude explains the robustness of the turbulent state in S3T: the streak grows relentlessly by lift-up due to the roll forcing by the perturbations resulting from the parametric instability of LV_1 which would cause the streak amplitude to diverge were it not for the even stronger transient growth of projections on the adjoint modes associated with incipient streak instability, which strongly damp the streak energy on the advective time scale, which is short compared to the instability time scale, producing a tightly controlled equilibrium statistical state [13].

VII. CONCLUSION

The S3T system is a statistical state dynamics closed at second order that has highly simplified dynamics and naturally self-sustains a turbulent state with restricted support in streamwise wavenumber so that S3T turbulence is dynamically and computationally an attractive system for studying the mechanism underlying maintenance of wall-turbulence. S3T system turbulence is in many aspects realistic and in particular it supports a realistic self-sustaining process. In this work we have exploited the simplicity of the self-sustaining process in S3T turbulence with the stochastic parameterization of the third cumulant set to zero to study the mechanisms underlying the maintenance and regulation of turbulence in this system. The mechanism maintaining the turbulence is a parametric growth process associated with the time-dependence of the streamwise mean flow streak component and consistently the resulting structure of the perturbation state is that of the first Lyapunov vector supported by the time-dependent streak. With inclusion of a stochastic excitation with zero energy injection parameterizing the perturbation–perturbation nonlinearity

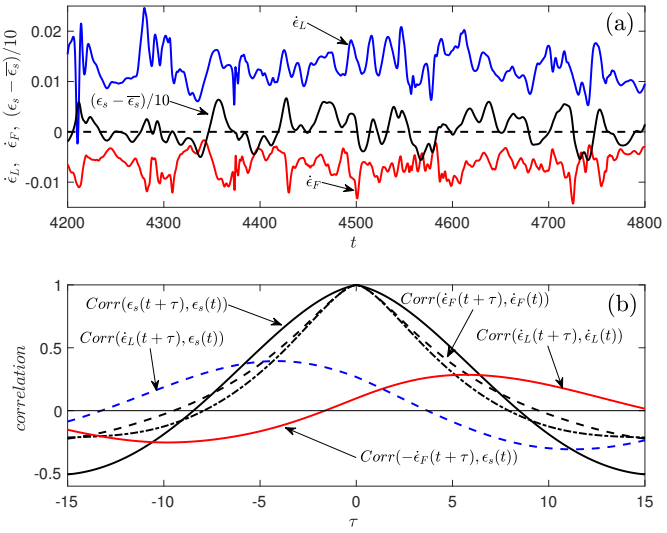

FIG. 17: Panel (a): Sample time series of the deviations from the time mean of the streak energy, $\epsilon_s - \overline{\epsilon_s}$, in an S3T simulation, of the contribution to the time rate of change in streak energy from mean advection (the lift-up mechanism), $\dot{\epsilon}_L$, which is always positive, and of the perturbation Reynolds stress, $\dot{\epsilon}_F$, which is always negative (cf. Appendix B). Panel (b): Comparison of the autocorrelations of the streak energy ϵ_s, of $\dot{\epsilon}_F$ and of $\dot{\epsilon}_L$. Shown also is the cross correlation of these quantities $Corr(-\dot{\epsilon}_F(t+\tau), \epsilon_s(t))$ and $Corr(\dot{\epsilon}_L(t+\tau), \epsilon_s(t))$. The cross correlation between ϵ_s and $-\dot{\epsilon}_F$ reveals that these quantities are closely positively correlated with only a $\tau = 5$ lead of the streak energy over the Reynolds stress term.

the perturbation field is supported by the first Lyapunov vector augmented by the remaining Lyapunov vectors which are induced to extract energy from the mean flow by the parameterized nonlinearity. The structure of the incoherent turbulence perturbations supported by the parametric growth process is shown to remain close to that of the Lyapunov vectors of the unforced example. Finally, the mechanism by which the statistical mean state is determined in S3T turbulence is identified to be a tight balance between robust streak growth by lift-up due to the roll forcing by the perturbations which in turn results from the parametric instability of the first Lyapunov vector (LV_1) and the even stronger damping resulting from transient growth of the adjoint modes which arise as the streak grows. These adjoint modes produce growth that increases rapidly near the stability boundary consistent with the slight amount of streak instability observed in the simulations [13]. These competing processes of robust streak growth opposed by strong damping produce a tightly controlled equilibrium statistical state.

Appendix A: Lyapunov exponents and vectors

Consider the time dependent linear dynamical system:

$$\dot{x} = \mathbf{A}(t)x \ , \tag{A1}$$

with x an n dimensional state vector and $\mathbf{A}$ a bounded $n \times n$ time dependent matrix. If the state of the system at time t_0 is $x(t_0)$, the state of the system at time t is given by

$$x(t) = \mathbf{\Phi}(t, t_0)\, x(t_0) \ , \tag{A2}$$

where the propagator, $\mathbf{\Phi}(t, t_0)$, is the $n \times n$ matrix that maps the state vector at time t_0 to the state vector at time t.

The Lyapunov exponents are defined to be the various limits

$$\lambda = \lim_{t\to\infty} \frac{\log \|\mathbf{\Phi}(t, t_0)\, x(t_0)\|}{(t - t_0)} \ , \tag{A3}$$

that can occur as x_0 spans the space of all possible initial conditions. We denote with $\|\cdot\|$ the norm chosen to measure the vector magnitude. The Lyapunov exponents are norm independent and also independent of the initial time t_0. Oseledets's theorem [42] guarantees that there are n such Lyapunov exponents $\lambda_1 > \lambda_2 > \cdots > \lambda_n$ (under the assumption that there is no degeneracy in the values of the Lyapunov exponents) that can be obtained as eigenvalues of the Hermitian positive matrix:

$$\mathbf{L}_\infty(t) = \lim_{t_0\to-\infty} \frac{\log\left(\mathbf{\Phi}(t, t_0)\mathbf{\Phi}^\dagger(t, t_0)\right)}{2(t - t_0)} \ . \tag{A4}$$

In the above definition the inner product is taken to be the dot product which is natural in our examples as our variables are velocities so the dot product results in a norm proportional to energy. We refer to the orthogo-

nal time dependent eigenvectors $u_1(t), u_2(t), \ldots, u_n(t)$ of $\mathbf{L}_\infty(t)$ as the Lyapunov vectors (LVs) of the system. With the exception of the first, these vectors depend on the chosen inner product consistent with their being orthogonal in that inner product (energy in our case). The time dependent eigenvector, $u_1(t)$, corresponding to the maximal Lyapunov exponent, λ_1, is called the first Lyapunov vector, LV_1.

Vectors proportional to LV_1, form subspace $E_1(t)$, and their magnitude changes with time as $t \to -\infty$ as $\exp(\lambda_1 t)$. LV_1 therefore becomes the dominant structure after a sufficiently long integration of the system (assuming no degeneracy of the first Lyapunov exponent). Vectors in the subspace $E_2(t)$ spanned by $u_1(t)$ and $u_2(t)$, except those that are proportional to $u_1(t)$, decay as $t \to -\infty$ as $\exp(\lambda_2 t)$ and $u_2(t)$ is referred to as the second Lyapunov vector, LV_2. In this way the state space is split into a set of nested subspaces $E_1(t) \subset E_2(t) \subset \cdots \subset E_n(t)$ such that the vectors that are in $E_i(t)$ and are not in subspace $E_{i-1}(t)$ decay as $t \to -\infty$ as $\exp(\lambda_i t)$. This definition of the Lyapunov vectors was introduced by Lorenz [43] in his studies of error growth in atmospheric dynamics; see also Farrell & Ioannou [40] and Wolfe & Samelson [48]. Assuming a physically based inner product, e.g. perturbation energy in our case, the orthogonal basis defined by these Lyapunov vectors provides a physically meaningful orthogonal basis for partitioning the state space of the evolving perturbations in the sense that perturbation states that were in the far past in a sphere of unit energy will evolve at time t into an ellipsoid the principle axes of which lie in the direction of the LV's and partition the state space into subspaces spanned by these vectors which are ranked in magnitude in the order of their Lyapunov exponents as $\exp(\lambda_i t)$.

It should be noted that the Lyapunov vector $u_i(t)$, with $i > 1$, when integrated forward will not in general grow asymptotically at rate λ_i (but almost surely at rate λ_1). This fact has two equally important roots. The first is mathematical: because of the orthogonalization procedure imposed on the Lyapunov vectors at each time step the components of the temporally evolving state vector growing at the rate of λ_i that lie in directions spanned by previous Lyapunov vectors LV_1 through LV_{i-1} is being projected out. While the orthogonal LV decomposition retains information on the subspace spanned by the Lyapunov vectors, it results in loss of the information on which structures are growing at the rate of each Lyapunov exponent at each time, with the exception of the first [51]. The second root is more physically relevant: from a physical perspective this follows from the fact that a random vector perturbation has measure zero probability of having zero projection on LV_1 and so any random perturbation results in growth that is asymptotically at rate λ_1. Besides being of profound physical significance, this universal property of all physical vectors asymptotically converging to LV_1 poses a problem for calculation of the Lyapunov vectors. In order to obtain the Lyapunov vectors operationally at all times we integrate forward the time dependent Lyapunov equation for the covariance (13) and after a sufficiently long integration the Lyapunov vectors at time t emerge as the eigenvectors of the covariance matrix $\mathbf{C}(t)$. The eigenvectors of $\mathbf{C}(t)$ define the Lyapunov vectors that are orthogonal in the energy inner product.

In some recent studies calculations were performed to determine at each time t the vectors that grow when integrated forward and decay when integrated backwards at the rate of the corresponding Lyapunov exponent [52]. These vectors, called confluent Lyapunov vectors (CLV), generalize to time dependent linear systems the eigenvector analysis of time independent linear systems [48, 53, 54]. However, the confluent Lyapunov vectors are not orthogonal in any physical norm. In order to use them to partition energy growth as we do in our analysis the additional step of orthogonalizing the CLV's in energy would have to be performed, which would serve to recover the LV's that we have discussed.

Appendix B: Streak Energetics

The streak component of the mean streamwise velocity, U, is defined as $U_\mathrm{s} = U - [U]_z$, where $[\cdot]_z$ denotes the spanwise average. The streak is the part of the streamwise velocity with zero x wavenumber but nonzero z wavenumber Fourier components. By subtracting (4a) from its spanwise average we obtain an equation for the evolution of the streak velocity:

$$\begin{aligned}\partial_t U_\mathrm{s} = &-\partial_y \left(UV - [UV]_z\right) - \partial_z \left(UW\right) \\ &- \partial_y \left([uv]_x - [uv]_{x,z}\right) - \partial_z \left([uw]_x\right) + \Delta U_\mathrm{s}/Re \ ,\end{aligned} \tag{B1}$$

using notation (2), and from (B1) we obtain the following evolution equation for the streak energy, $\epsilon_s \equiv \int_{-1}^{1} \left[U_s^2/2\right]_z \, \mathrm{d}y$:

$$\dot{\epsilon}_s = \dot{\epsilon}_L + \dot{\epsilon}_F + \dot{\epsilon}_D \ , \tag{B2}$$

where

$$\dot{\epsilon}_L = -\int_{-1}^{1} \Big[U_\mathrm{s} \left(V\partial_y U + W\partial_z U\right)\Big]_z \, \mathrm{d}y \, , \tag{B3}$$

is the contribution to the streak energy rate of growth from advection of mean U momentum by the V and W velocities. The term

$$\dot{\epsilon}_F = -\int_{-1}^{1} \Big[U_\mathrm{s}\partial_y \left([uv]_x\right) + U_\mathrm{s}\partial_z \left([uw]_x\right)\Big]_z \, \mathrm{d}y \, , \tag{B4}$$

is the contribution to the streak energy rate of growth from the perturbation Reynolds-stress divergence, and

$$\dot{\epsilon}_D = \frac{1}{Re}\int_{-1}^{1} \left[U_\mathrm{s} \, \Delta U_\mathrm{s}\right]_z \, \mathrm{d}y \ , \tag{B5}$$

is the rate of dissipation of streak energy.

ACKNOWLEDGMENTS

This work was initiated during the 2013 First Multiflow Summer Workshop at the Universidad Politécnica de Madrid with financial support from the Multiflow Program of the European Research Council. We would like to thank Prof. Javier Jiménez, Prof. Dennice Gayme, Dr. Vaughan Thomas, Dr. Adrián Lozano-Durán and Dr. Navid Constantinou for useful comments and fruitful discussions. Brian Farrell was partially supported by NSF AGS-1246929.

[1] S. J. Kline, W. C. Reynolds, F. A. Schraub, and P. W. Runstadler, J. Fluid Mech. **30**, 741 (1967).
[2] K. M. Butler and B. F. Farrell, Phys. Fluids **4**, 1637 (1992).
[3] S. C. Reddy and D. S. Henningson, J. Fluid Mech. **252**, 209 (1993).
[4] M. T. Landahl, J. Fluid Mech. **98**, 243 (1980).
[5] J. D. Swearingen and R. F. Blackwelder, J. Fluid Mech. **182**, 255 (1987).
[6] H. P. Bakewell Jr. and L. Lumley, Phys. Fluids **10**, 1880 (1967).
[7] F. Waleffe, Stud. Appl. Math. **95**, 319 (1995).
[8] K. Hamilton, J. Kim, and F. Waleffe, J. Fluid Mech. **287**, 317 (1995).
[9] F. Waleffe, Phys. Fluids **9**, 883 (1997).
[10] P. Hall and S. Sherwin, J. Fluid Mech. **661**, 178 (2010).
[11] W. Schoppa and F. Hussain, J. Fluid Mech. **453**, 57 (2002).
[12] B. F. Farrell and P. J. Ioannou, Phys. Fluids A **5**, 1390 (1993).
[13] B. F. Farrell and P. J. Ioannou, J. Fluid Mech. **708**, 149 (2012).
[14] B. F. Farrell, D. F. Gayme, and P. J. Ioannou, Phil. Trans. R. Soc. A (2016), (submitted, arXiv:1609.06769).
[15] E. Hopf, J. Ration. Mech. Anal. **1**, 87 (1952).
[16] R. H. Kraichnan, Phys. Fluids **7**, 1048 (1964).
[17] U. Frisch, *Turbulence: The Legacy of A. N. Kolmogorov* (Cambridge University Press, 1995).
[18] B. F. Farrell and P. J. Ioannou, J. Atmos. Sci. **64**, 3652 (2007).
[19] K. Srinivasan and W. R. Young, J. Atmos. Sci. **69**, 1633 (2012).
[20] S. M. Tobias and J. B. Marston, Phys. Rev. Lett. **110**, 104502 (2013).
[21] N. C. Constantinou, B. F. Farrell, and P. J. Ioannou, J. Atmos. Sci. **71**, 1818 (2014).
[22] J. R. Herring, J. Atmos. Sci. **20**, 325 (1963).
[23] J. R. Herring, J. Atmos. Sci. **21**, 277 (1964).
[24] B. F. Farrell and P. J. Ioannou, J. Atmos. Sci. **60**, 2101 (2003).
[25] B. F. Farrell and P. J. Ioannou, J. Atmos. Sci. **66**, 2444 (2009).
[26] B. F. Farrell and P. J. Ioannou, J. Atmos. Sci. **66**, 3197 (2009).
[27] J. B. Parker and J. A. Krommes, New J. Phys. **16**, 035006 (2014).
[28] N. A. Bakas and P. J. Ioannou, Phys. Rev. Lett. **110**, 224501 (2013).
[29] W. V. R. Malkus, Proc. Roy. Soc. A. **225**, 196 (1954).
[30] W. V. R. Malkus and G. Veronis, J. Fluid Mech. **1**, 521 (1956).
[31] W. C. Reynolds and W. G. Tiederman, J. Fluid Mech. **27**, 253 (1967).
[32] W. V. R. Malkus, J. Fluid Mech. **1**, 521 (1956).
[33] N. C. Constantinou, A. Lozano-Durán, M.-A. Nikolaidis, B. F. Farrell, P. J. Ioannou, and J. Jiménez, J. Phys. Conf. Ser. **506**, 012004 (2014).
[34] J. U. Bretheim, C. Meneveau, and D. F. Gayme, Phys. Fluids **27**, 011702 (2015).
[35] B. F. Farrell, P. J. Ioannou, J. Jiménez, N. C. Constantinou, A. Lozano-Durán, and M.-A. Nikolaidis, J. Fluid Mech. **809**, 290 (2016).
[36] P. Hall and F. Smith, J. Fluid Mech. **227**, 641 (1991).
[37] K. Deguchi, P. Hall, and A. Walton, J. Fluid Mech. **721**, 58 (2013).
[38] J. Jiménez, Phys. Fluids **25**, 101302 (2013).
[39] P. G. Drazin and W. H. Reid, *Hydrodynamic Stability* (Cambridge University Press, Cambridge, 1981).
[40] B. F. Farrell and P. J. Ioannou, J. Atmos. Sci. **53**, 2041 (1996).
[41] B. F. Farrell and P. J. Ioannou, J. Atmos. Sci. **56**, 3622 (1999).
[42] V. I. Oseledets, Trans. Moscow Math. Soc. **19**, 197 (1968).
[43] E. N. Lorenz, Physica D **13**, 90 (1984).
[44] V. Thomas, B. F. Farrell, P. J. Ioannou, and D. F. Gayme, Phys. Fluids **27**, 105104 (2015).
[45] P. J. Schmid and D. S. Henningson, *Stability and Transition in Shear Flows* (Springer, New York, 2001).
[46] V. Thomas, B. K. Lieu, M. R. Jovanović, B. F. Farrell, P. J. Ioannou, and D. F. Gayme, Phys. Fluids **26**, 105112 (2014).
[47] B. F. Farrell and P. J. Ioannou, J. Atmos. Sci. **53**, 2025 (1996).
[48] C. Wolfe and R. Samelson, Tellus A **59**, 355 (2007).
[49] B. F. Farrell and P. J. Ioannou, Stoch. Dyn. **2**, 395 (2002).
[50] B. F. Farrell and P. J. Ioannou, J. Atmos. Sci. **59**, 2647 (2002).
[51] H.-l. Yang and G. Radons, Phys. Rev. E **82**, 046204 (2010).
[52] X. Ding, H. Chaté, P. Cvitanović, E. Siminos, and K. A. Takeuchi, Phys. Rev. Lett. **117**, 024101 (2016).
[53] F. Ginelli, P. Poggi, A. Turchi, H. Chaté, R. Livi, and A. Politi, Phys. Rev. Lett. **99**, 130601 (2007).
[54] H.-l. Yang and G. Radons, Phys. Rev. Lett. **108**, 154101 (2012).